Impact of Torsional and Conformational Flexibility on Pedal Motion and Thermal Expansion in Pyridyl Bisimine Cocrystals

Navkiran Juneja,^a Daniel K. Unruh,^a Gary C. George III,^a and Kristin M. Hutchins^a*

^aDepartment of Chemistry and Biochemistry, Texas Tech University, 1204 Boston Avenue, Lubbock, Texas 79409, United States. Email: kristin.hutchins@ttu.edu

ABSTRACT

The impact of intermolecular interactions and molecular motion on solid-state properties is an active field of interest for chemists and materials scientists. For example, cocrystallization has been shown to modify and/or enhance the solid-state behaviors of a molecule when compared to the single-component solid. Here, we describe a series of cocrystals containing bis(pyridin-4-ylmethylene)benzene-1,4-diamine (**BPDI**) and ditopic or tritopic hydrogen-bond-donor molecules that are conformationally flexible. The components in all the cocrystals self-assemble through hydroxyl-pyridine heterosynthons to afford one-dimensional chains due to the conformations of the donor molecules. **BPDI** is torsionally flexible, and in cocrystals with ditopic hydrogen-bond donors the molecule is almost planar whereas, in cocrystals with tritopic hydrogen-bond donors, **BPDI** is significantly twisted. This twisting in **BPDI** affects crystal packing and affords higher

thermal expansion coefficients. Cocrystallization of **BPDI** with resveratrol, another torsionallyflexible molecule, induces molecular pedal motion in **BPDI** and results in larger expansion behavior in the cocrystal.

INTRODUCTION

Cocrystallization, a process of synthesizing multi-component solids based on well-defined supramolecular interactions, 1, 2 has gained an immense amount of interest and importance in the past two decades.³⁻⁵ The use of crystal engineering to design cocrystals by modifying the molecular components (e.g., co-formers), noncovalent interactions, and, ultimately, solid-state properties, continues to be an ongoing area of research for materials scientists. ⁶⁻¹¹ Incorporating functionalities that impart specific behaviors to the overall solid can be useful for enhancing physicochemical behaviors. Non-covalent interactions, specifically hydrogen bonds, are one of the most frequently employed interactions in crystal engineering and cocrystallization because of their strength and directionality. Specifically, solids incorporating benzoic acids or phenols as hydrogen-bond donors and pyridines as hydrogen-bond acceptors are some of the most-studied complexes. 12-18 Energy calculations have been performed to quantify noncovalent interaction strengths in such complexes. 19, 20 For example, quantum mechanical calculations have shown that formation of heterosynthons in molecular crystals can be more favorable than homosynthons,21 and the supramolecular synthon energy for a hydroxyl-pyridine heterosynthon has been calculated to be ca. 30 kJ/mol.²² The robustness of the hydroxyl-pyridine (O-H···N) synthon has been utilized to template synthesis of pyridine-containing macrocycles, 23 enforce topochemical alignment of olefins for photoreactions, 24-27 and construct liquid crystals with photoswitchable properties, 28

among others. Although the hydroxyl-pyridine synthon is robust, it still remains challenging to control the extended solid-state packing of molecular assemblies. Use of molecular building blocks or tectors containing functional groups that recognize each other and facilitate self-assembly and formation of networks is one strategy that has been used to predict and control supramolecular structures.²⁹ However, introduction of moieties that are conformationally flexible can affect crystal packing, as well as the intermolecular interactions formed in the solid state.³⁰

One solid-state property that our group and others have shown to be influenced by hydrogenbonding interactions in cocrystals is thermal expansion (TE).³¹⁻³⁴ TE describes how a solid experiences changes uniaxially or volumetrically in response to temperature alterations. TE properties can be modified by incorporating different molecules into the solid, which changes the crystal packing and/or intermolecular interactions. Most solids experience positive TE (PTE), or expansion upon heating,³⁵ whereas the behavior of contraction upon heating is unusual and termed negative TE (NTE). 36, 37 Recently, uniaxial NTE has been observed in some organic materials. 35, ³⁸ Understanding TE behaviors of materials is important in designing electronic devices such as organic semiconductors and within engineering fields. However, the ability to alter and control TE properties in multi-component solids continues to be highly challenging for material scientists since the behavior depends on multiple structural characteristics. Colossal TE behaviors ($\alpha \ge 100$ MK⁻¹)³⁹ have been achieved in solids containing functional groups that undergo solid-state motion.^{35,40-42} For example, dynamic solid-state pedal motion has been observed in molecules with azo (N=N), ethylene (C=C), and imine (C=N) functional groups attached to aromatic rings^{43, 44} and has been shown to afford colossal TE. 6, 31, 45 Multi-component solids that include co-formers functionalized with azo and olefin groups have also been reported to exhibit pedal motion, as confirmed by variations in the molecular conformations with temperature. 46, 47 Imines are a

broadly-studied class of organic compounds because of their straightforward synthesis via acid-catalyzed condensation of primary amines with aldehydes. In Schiff-base compounds, imines frequently undergo enol-keto tautomerism, which depends on molecular motion ability, proton transfer, and overall crystal packing. ⁴⁸⁻⁵⁰ Imines also exhibit torsional flexibility ⁵¹ and often crystallize in non-planar geometries, which impacts extended crystal packing. ^{49, 52} We recently investigated the solid-state properties of molecules containing one imine group and showed that the torsional flexibility affords unique TE properties. ⁵³ Imine-based molecules have frequently been used as ligands in metal-organic frameworks ^{54, 55} and as components within covalent-organic frameworks; ⁵⁶⁻⁵⁹ however, cocrystals containing imines are less explored. ⁶⁰ Thus, we were motivated to design and synthesize hydrogen-bonded cocrystals featuring imine functional groups, with the goal of investigating torsional flexibility, dynamic pedal motion, and impacts on TE properties.

We selected a molecule containing two imine groups, namely, bis(pyridin-4-ylmethylene)benzene-1,4-diamine (BPDI) (Figure 1). As a single-component solid, BPDI is torsionally flexible and the pyridyl and benzyl rings lie twisted in the solid state. Four hydrogen-bond-donor molecules containing either two or three hydroxyl groups were used as co-formers to target synthesis of cocrystals with different dimensionalities. Interestingly, one-dimensional hydrogen-bonded assemblies formed in all cases due to the conformational flexibility of the hydroxyl groups (*syn-syn*, *anti-anti*, or *syn-anti*) (Figure 2). Moreover, pedal motion within BPDI was only observed in the cocrystal with resveratrol, wherein both components are actually motion capable. The cocrystal of BPDI and resveratrol also exhibited the largest uniaxial TE coefficient within the series.

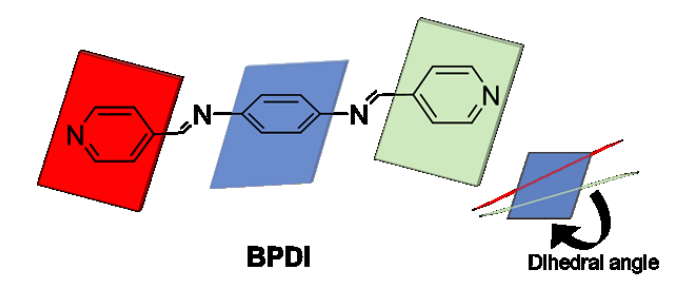


Figure 1. Torsional flexibility in **BPDI**. The planes of the two pyridine rings (which may or may not be coplanar) are shown with red and green, while the phenyl ring is shown in blue. The dihedral angle is the angle between the red and blue planes or the green and blue planes.

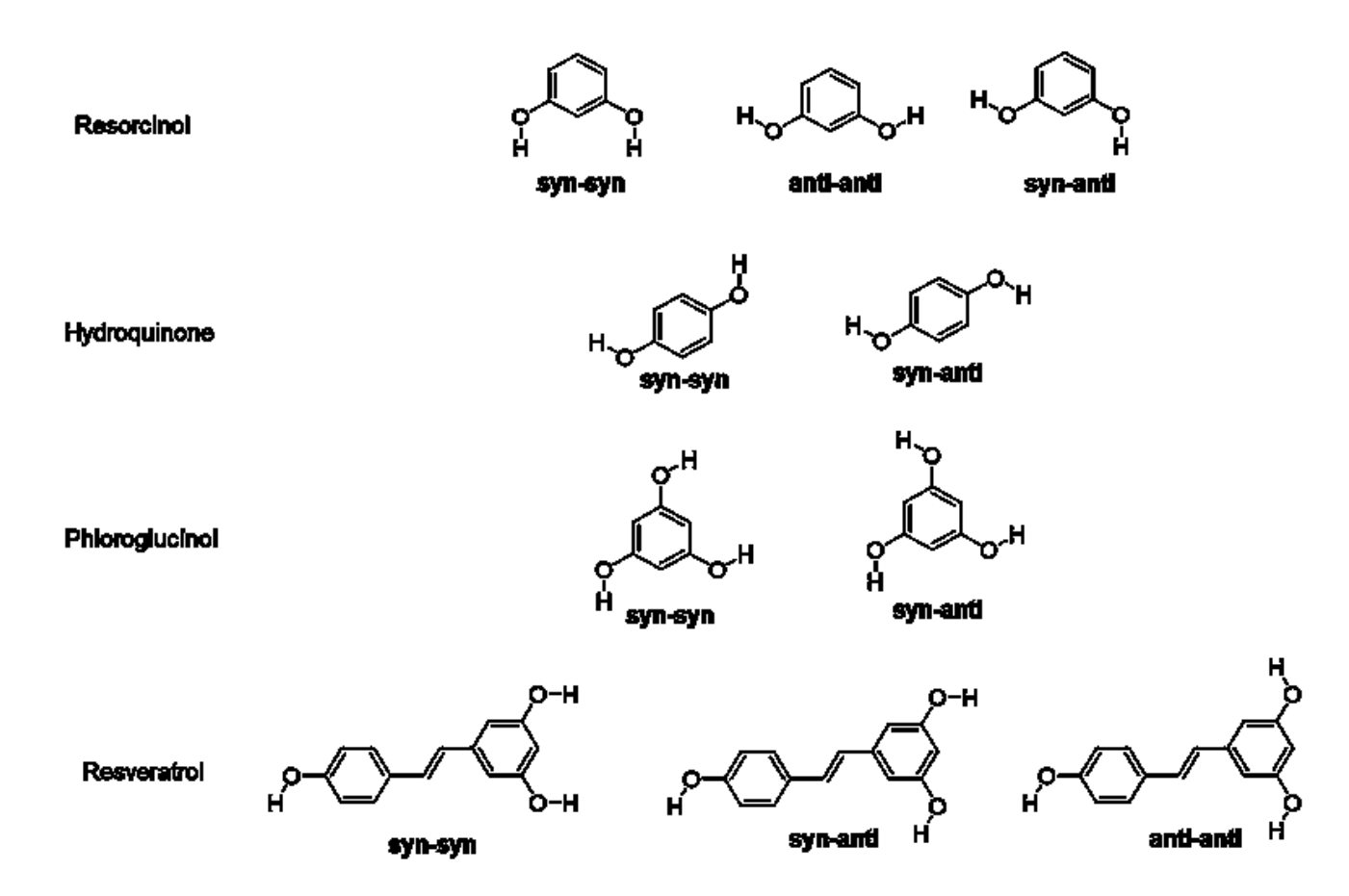
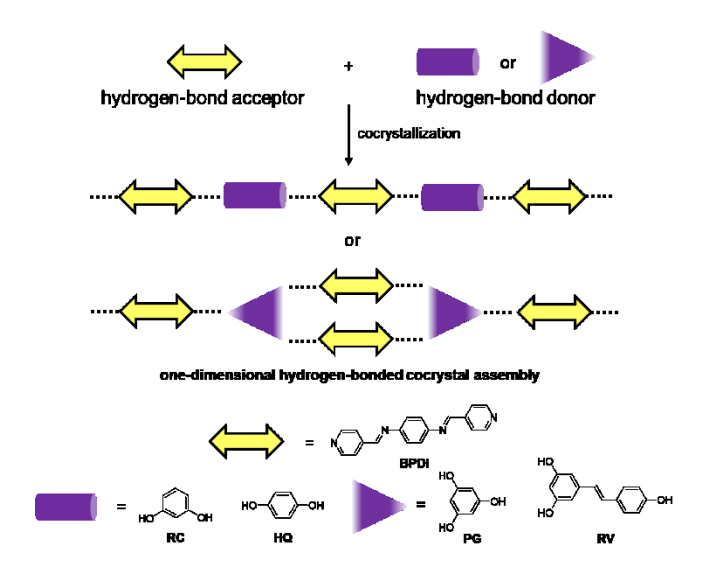


Figure 2. Hydrogen-bond-donor molecules in this study depicting conformational flexibility in the hydroxyl groups.

EXPERIMENTAL

We selected the ditopic hydrogen-bond-donor molecules resorcinol (**RC**) and hydroquinone (**HQ**), as well as the tritopic donor molecules phloroglucinol (**PG**) and resveratrol (**RV**). All four donors contain hydroxyl groups connected to aromatic rings (Scheme 1). The hydrogen-bond acceptor, **BPDI**, was synthesized mechanochemically using a Form-Tech Scientific FTS1000 shaker mill following a reported method,⁶¹ with the addition of a purification step via recrystallization in methanol (see SI for details). Single crystals of **BPDI** and each cocrystal were grown using slow evaporation methods (see SI for details). Variable-temperature single-crystal X-ray diffraction (VT SCXRD) experiments were performed for each solid over the temperature range of 290-190 K in 20 K intervals (Table S1-S10). The bulk crystalline material was characterized by ¹H NMR spectroscopy (Figure S9-S13) and powder X-ray diffraction (PXRD).

Scheme 1. Formation of 1D hydrogen-bonded assemblies within cocrystals containing **BPDI**. The O-H···N hydrogen bonds are represented by dotted lines.



RESULTS AND DISCUSSION

Characterization

The PXRD data was obtained by gently grinding single crystals of **BPDI** or the cocrystals, and in each case, showed good correlation with the simulated PXRD pattern obtained from SCXRD data at 290 K (Figure S14-S18). The components of **RC·BPDI** and **HQ·BPDI** crystallize in a 1:1 molar ratio, while components within **PG2·BPDI3** and **RV2·BPDI3** crystallize in a 2:3 molar ratio as confirmed by SCXRD data and ¹H NMR spectroscopy.

X-ray crystal structure analysis

The single crystal structure of **BPDI** has been reported at 298 K. 61, 62 We obtained isostructural crystals here, and conducted the VT SCXRD study over the temperature range of 190-290 K. Over this range, **BPDI** did not show evidence of solid-state pedal motion (i.e., disorder) as a singlecomponent solid. **BPDI** has also been demonstrated to crystallize as various hydrates, ^{61,63} but here, we only focus on the anhydrous form. To compare to the cocrystals, we will briefly discuss the structural characteristics of **BPDI**. **BPDI** crystallized in the centrosymmetric, triclinic space group $P\overline{1}$ and the asymmetric unit contains half of two crystallographically unique molecules. The two crystallographically unique molecules adopt a non-planar conformation due to the torsional flexibility of the imine group (Figure 3a). The dihedral angles between the pyridine and phenyl rings in the two unique molecules are 53° and 59° at 290 K. Neighboring molecules interact via long C-H···N(pyr) hydrogen bonds (3.433(2) Å at 290 K) to form one-dimensional (1D) chains. Each chain includes both crystallographically unique molecules, which alternate in an ABAB fashion (Figure 3b, A and B are the molecules with N3 and N1, respectively). The adjacent chains interact via $C-H(\alpha)\cdots N(pyr)$ contacts to form a sheet-like structure. The imine groups engage in C-H(imine)···N(imine) weak hydrogen bonds that lie in parallel with the aromatic C- $H(pyr)\cdots\pi(benz)$ forces between the sheets. There are also two types of face-to-face $\pi\cdots\pi$ interactions present, as a result of A and B type molecules between the sheets.

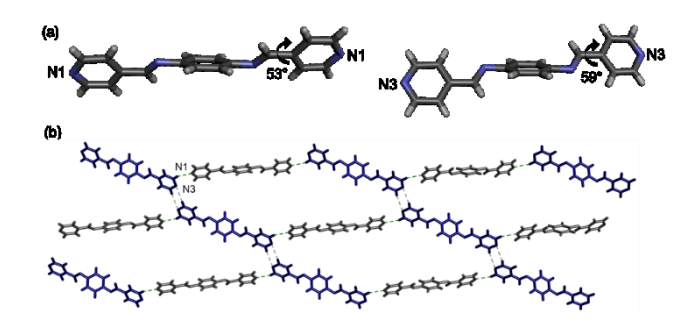


Figure 3. X-ray crystal structures of **BPDI** at 290 K highlighting: a) two crystallographically unique half molecules with dihedral angles and b) extended packing of the 1D chains.

Cocrystallization of **BPDI** with the ditopic donors **RC** or **HQ** afforded the cocrystals **RC·BPDI** or **HQ·BPDI**. The components within both cocrystals crystallized in the monoclinic, centrosymmetric space group P21/n in a molar ratio of 1:1. The asymmetric unit of **RC·BPDI** consists of one molecule of **BPDI** and one molecule of **RC**, whereas the asymmetric unit of **HQ·BPDI** contains half a molecule of **BPDI** and half a molecule of **HQ**. The **BPDI** molecule within both solids crystallizes in a nearly planar geometry, with a dihedral angle between the benzene ring and the pyridine rings of 5° and 10° in **RC·BPDI** (Figure S1a) and 10° in **HQ·BPDI** (Figure S1b). The two molecules within **RC·BPDI** interact via two unique O-H···N hydrogen bonds (2.759(2) Å and 2.803(2) Å), while in **HQ·BPDI** there is only one unique O-H···N hydrogen bond (2.771(2) Å).

The hydroxyl groups within **RC** can exist in three conformations, *syn-syn*, *syn-anti*, and *anti-anti* (Figure 2). Nearly all of the reported cocrystals of bipyridines with **RC** exhibit zero-dimensional (0D) assemblies with **RC** in the *syn-syn* conformation. ^{26, 32, 64-66} One exception was reported by MacGillivray and coworkers, where 1D chains form because **RC** adopts the *anti-anti* conformation. ⁶⁷ Although we expected **BPDI** and **RC** to self-assemble into a 0D assembly, the components unexpectedly arrange into 1D chains because **RC** crystallizes in the *anti-anti* conformation (Figure 4a). Within the chain, every other pair of **RC** and **BPDI** molecules are

rotated by 59°. In **HQ·BPDI**, the **HQ** component adopts the *syn-anti* conformation and also affords a 1D hydrogen-bonded chain (Figure 4b). In both cocrystals, adjacent chains interact via C-H(pyr)···O interactions to form a sheet. Neighboring sheets stack approximately along the b axis in **RC·BPDI**, and the sheets interact via offset π ··· π interactions, C-H··· π interactions between **BPDI** molecules, and C-H···O interactions between **RC** molecules. In **HQ·BPDI**, the sheets stack along the c axis in an ABAB fashion, where A and B are rotated by 59° and interact through C-H··· π and C-H···O interactions between **BPDI** and **HQ** molecules.

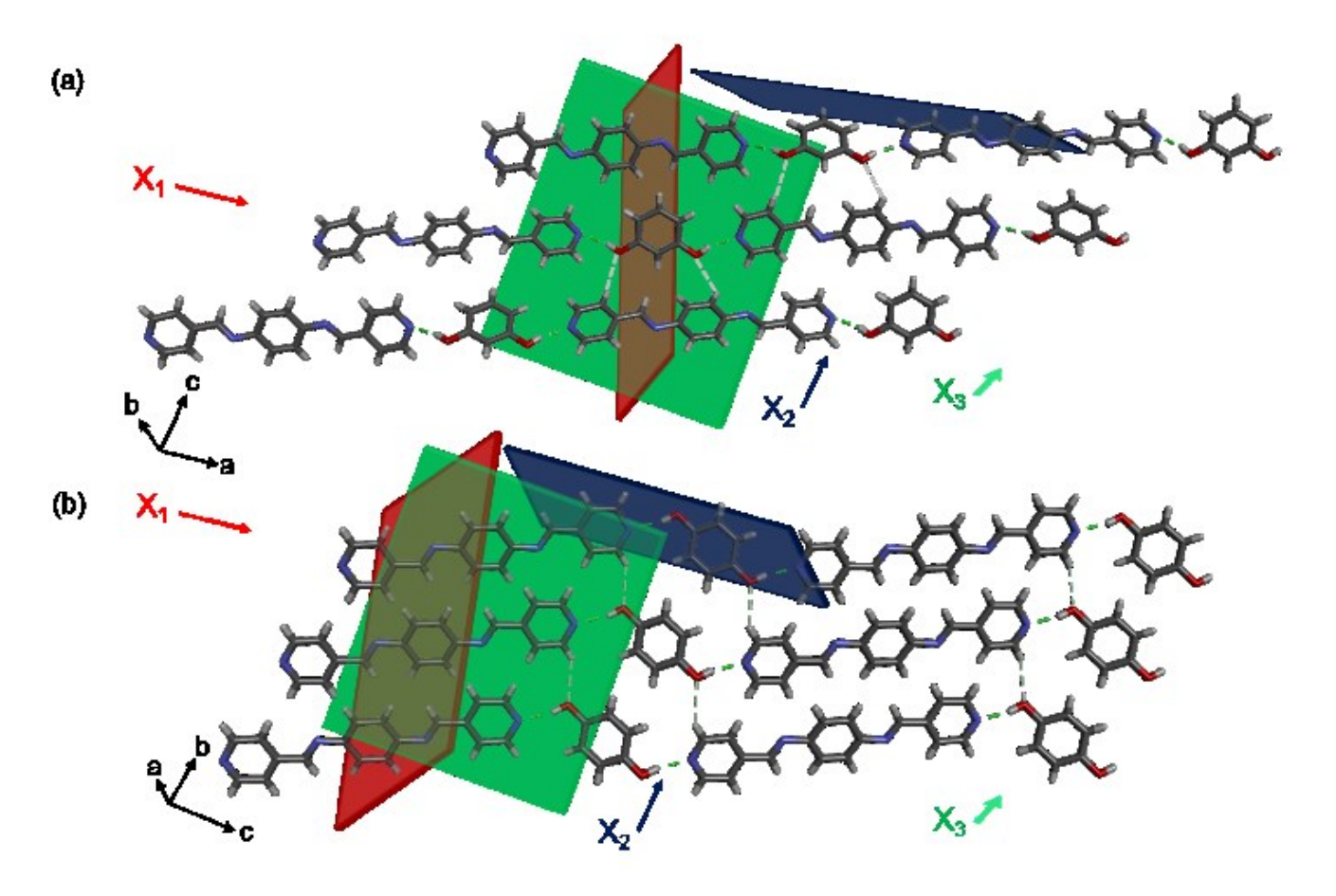


Figure 4. Crystal structures of (a) **RC·BPDI** and (b) **HQ·BPDI** showing packing of 1D hydrogen-bonded chains. The O-H···N bonds are shown in green and C-H···O interactions in grey. The TE axes are highlighted by the included planes and arrows with X_1 in red, X_2 in dark blue, and X_3 in green.

Cocrystallization of **BPDI** with the tritopic donor molecules, **PG** or **RV**, afforded the cocrystals $PG_2 \cdot BPDI_3$ or $RV_2 \cdot BPDI_3$. The components of both solids crystallize in the triclinic, centrosymmetric space group $P\overline{1}$ in a molar ratio of 2:3 (donor:BPDI). The asymmetric unit of $PG_2 \cdot BPDI_3$ contains two crystallographic unique molecules of **PG**, two unique molecules of **BPDI**, and two unique half molecules of **BPDI**. Thus, two **BPDI** molecules are symmetrical and two are unsymmetrical. The symmetrical **BPDI** molecules exhibit dihedral angles of 27° and 31°, while the unsymmetrical **BPDI** molecules exhibit dihedral angles of 42° and 63° within one **BPDI** molecule and 31° and 24° within the other **BPDI** molecule (Figure S2a). The asymmetric unit of $RV_2 \cdot BPDI_3$ consists of one crystallographically unique RV molecule, one unique molecule of **BPDI**, and one unique half molecule of **BPDI**. Thus, one of the **BPDI** molecules is symmetrical and the other is unsymmetrical. The symmetrical **BPDI** molecule exhibits a dihedral angle of 37°, while the unsymmetrical **BPDI** molecule exhibits dihedral angles of 47° and 75° (Figure S2b).

We envisioned that the tritopic donors could facilitate formation of 1D chains or 2D sheets, as both structural types have been reported with these donors.⁶⁸⁻⁷² In the cocrystals of **BPDI** and **PG** or **RV**, the hydrogen-bond donors adopt the *syn-syn* conformation and form infinite 1D arrays via strong O-H···N hydrogen bonds. Within each chain, due to the *syn-syn* conformation, two donors organize two identical **BPDI** molecules into stacked dimer. The remaining third hydroxyl group engages in a hydrogen bond with a symmetrical **BPDI** molecule (Figure 5).

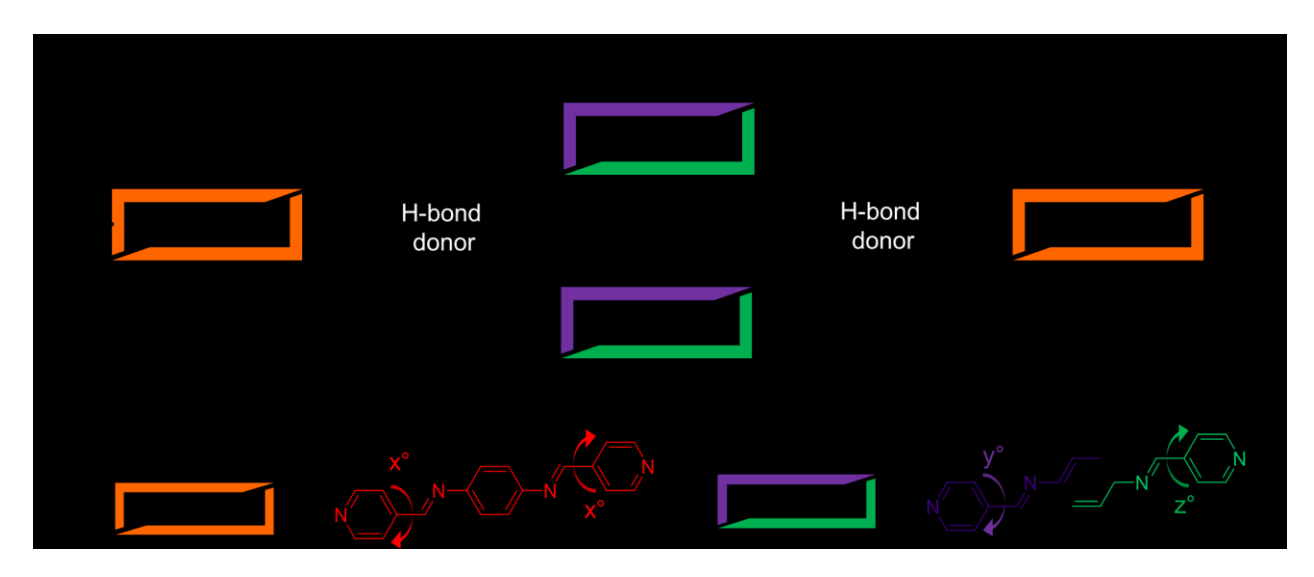


Figure 5. Depiction of the 1D arrays formed by the tritopic hydrogen-bond-donor molecules, **PG** and **RV**.

For $PG_2 \cdot BPDI_3$, adjacent 1D chains are stacked in an ABAB fashion, as a result of the two unique PG molecules. Within the stacked BPDI molecules, the ABAB pattern results from a BPDI dimer (A) and a single BPDI (B). The 1D chains interact via C-H···O interactions between PG molecules, $\pi \cdots \pi$ interactions between BPDI molecules, and C-H··· π interactions between BPDI molecules to form a sheet (Figure 6a). The sheets form stacks via C-H··· π interactions between BPDI and PG molecules, C-H···N interactions between BPDI molecules, and C-H···O interactions between BPDI and PG molecules (Figure S25).

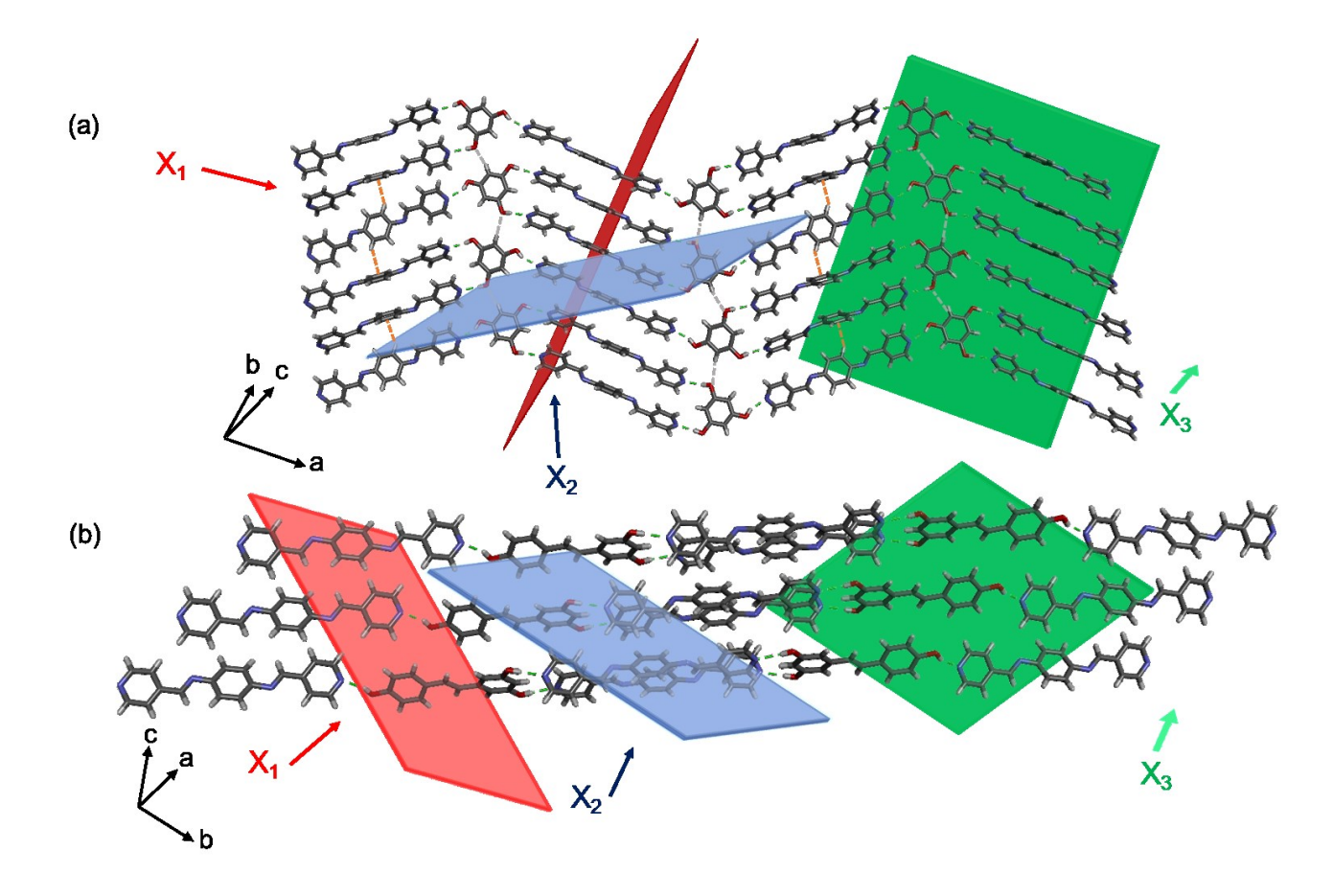


Figure 6. Crystal structures of (a) $PG_2 \cdot BPDI_3$ and (b) $RV_2 \cdot BPDI_3$ showing packing of 1D hydrogen-bonded arrays. The O-H···N bonds are shown in green, C-H···O interactions in grey, and C-H··· π interactions in yellow. The TE axes are highlighted by the included planes and arrows with X_1 in red, X_2 in dark blue, and X_3 in green. Disorder in **BPDI** in part b has been omitted for clarity.

Within $\mathbf{RV_2} \cdot \mathbf{BPDI_3}$, the adjacent 1D chains interact via C-H···O forces between \mathbf{BPDI} and \mathbf{RV} molecules, C-H··· π interactions between \mathbf{BPDI} molecules, and C-H··· π between \mathbf{BPDI} and \mathbf{RV} molecules to form a sheet (Figure 6b, Figure S29). The sheets self-assemble into stacks via C-H··· π and C-H···O interactions between \mathbf{BPDI} and \mathbf{RV} molecules (Figure S26). As a single-component solid, \mathbf{RV} is polymorphic due to its torsional flexibility. 73, 74 Within $\mathbf{RV_2} \cdot \mathbf{BPDI_3}$, the

RV molecule exhibits a dihedral angle of 26°. Moreover, half of the unsymmetrical **BPDI** molecule is disordered over two sites, and the site occupancies for the two conformations vary over the temperature range of 190-290 K, indicating molecular pedal motion in the cocrystal (Table 1, Figure S27). Interestingly, incorporating a torsionally-flexible co-former turned pedal motion on in **BPDI**.

Table 1. Site occupancies of the major conformation within half of the **BPDI** molecule in **RV₂·BPDI₃** as a function of temperature. The error is denoted in the parentheses.

Temperature (K)	Major conformation site occupancy (%)		
190	97 (1)		
210	94 (1)		
230	91 (1)		
250	87 (1)		
270	83 (1)		
290	80 (1)		

Thermal expansion behaviors

To investigate the effects of torsional flexibility, crystal packing, and motion on the TE properties of the 1D hydrogen-bonded cocrystals, the TE coefficients (α_{X_1} , α_{X_2} , and α_{X_3}) and the principal axes of TE (X_1 , X_2 , and X_3) were calculated using the software, PASCal⁷⁵ (Table 2). Along X_1 in **BPDI** and the four cocrystals, uniaxial zero TE or NTE occurs along the direction of the strongest hydrogen bonds within each solid. Mild or moderate PTE occurs along X_2 , and

colossal or near colossal PTE occurs along X_3 in **BPDI** and all the cocrystals. The volumetric TE coefficient for each cocrystal is lower than that of **BPDI** because the components are held together by stronger hydrogen bonds.

Table 2. TE coefficients for the crystals with errors denoted in the parentheses and approximate crystallographic axes denoted in brackets.

Crystal	α_{X_1} (MK ⁻¹)	α_{X_2} (MK ⁻¹)	$\alpha_{X_3}(MK^{-1})$	$\alpha_V(MK^{-1})$
	[axis]	[axis]	[axis]	
BPDI	0(1)	40 (1)	152 (1)	192 (2)
	[-2 -1 3]	[-1 1 0]	[-3 -1 -1]	
RC·BPDI	-4 (1)	66 (1)	111 (3)	174 (4)
	[-1 0 0]	[0 0 1]	[0 -1 0]	
HQ·BPDI	-17 (1)	46 (1)	155 (2)	184 (3)
	[1 0 7]	[0 -1 0]	[-1 0 0]	
PG ₂ ·BPDI ₃	-5 (2)	66 (1)	94 (2)	155 (1)
	[-2 0 -1]	[2 -3 0]	[-1 -1 1]	
RV ₂ ·BPDI ₃	-25 (2)	29 (1)	172 (5)	177 (2)
	[5 1 0]	[-3 2 1]	[1 -2 3]	

Two of the four cocrystals exhibit more significant NTE along X_1 . In **HQ·BPDI** (α_{X_1} = -17 MK⁻¹), the NTE is due to a decrease in the *c*-axis length upon heating, which coincides with the 1D hydrogen-bonded chains and a decrease in the length of the **BPDI** molecule upon heating. **RV**₂·**BPDI**₃ exhibits NTE along X_1 (α_{X_1} = -25 MK⁻¹) due to a contraction of the *a* axis upon heating, as well as a shortening between neighboring **RV** molecules by 0.03 Å upon heating from 190 to 290 K.

The intermolecular interactions that contribute to the PTE along X_2 are the C-H···O interactions that hold neighboring 1D chains together and facilitate formation of the sheets. For the cocrystals with tritopic donors, **PG₂·BPDI₃** and **RV₂·BPDI₃**, C-H··· π and offset π ··· π interactions between stacked **BPDI** molecules also contribute to the PTE along X_2 (Figure S32, S33). The cocrystal

RV₂·BPDI₃ exhibits less expansion due to some contribution from the strong hydrogen bonds to the X₂ axis (Figure 6b). The coefficients for **RV₂·BPDI₃** along X₁ and X₂ are -25 MK⁻¹ and 29 MK⁻¹, respectively; thus, the coefficients nearly cancel each other out, resulting in unique two-dimensional zero TE behavior.

Three of the four cocrystals exhibit 'colossal' TE along X₃, and for all four cocrystals, the X₃ axis lies along the direction that the sheets are stacked. In the cocrystals containing ditopic donors, the TE coefficient is higher for HQ·BPDI than RC·BPDI. In HQ·BPDI, neighboring sheets are rotated by ca. 60° , and the stacking of sheets is facilitated through t-shaped, C-H··· π interactions. In **RC·BPDI**, the sheets are stacked in a parallel fashion and interact via offset $\pi \cdots \pi$ interactions. The weaker, t-shaped, C-H $\cdots\pi$ interactions in **HQ·BPDI** undergo a larger change with temperature $(\Delta = 0.06 \text{ Å})$ when compared to the $\pi \cdots \pi$ interactions in **RC·BPDI** ($\Delta = 0.04 \text{ Å}$) (Figure S30-S31). In the solids containing tritopic donors, PG2·BPDI3 experiences nearly colossal PTE and **RV₂·BPDI₃** exhibits the largest TE coefficient along X_3 within the series. Along X_3 , the C-H··· π interactions and C-H···N(pyr) interactions in **PG₂·BPDI₃** undergo a smaller increase ($\Delta = 0.04 \text{ Å}$) when compared to the C-H··· π (benz) interactions within the sheet and C-H···O interactions between sheets in RV₂·BPDI₃ ($\Delta = 0.06$ Å) (Figure S32-S33). Furthermore, for RV₂·BPDI₃, X₃ also lies along the direction where pedal motion occurs and the pyridine ring twisting in the unsymmetrical **BPDI** molecule, and hence the motion along with twisting contributes to the colossal PTE (Figure S28).

The dihedral angles within the **BPDI** molecules are larger in the cocrystals containing tritopic hydrogen-bond-donor molecules as compared to the ones with ditopic hydrogen-bond donors. The near planar geometry of the **BPDI** molecule in the cocrystals with ditopic donors results in sheets and stacks that are relatively planar. However, the twisting of the **BPDI** molecule in the cocrystals

with tritopic donors results in sheets and stacks that contain edge-to-face and/or twisted molecules. The torsional flexibility and twisting affect the X_2 axis in $PG_2 \cdot BPDI_3$ and the X_3 axis in $RV_2 \cdot BPDI_3$.

CONCLUSION

A series of hydrogen-bonded cocrystals were designed and synthesized and feature a hydrogenbond acceptor molecule containing two imine functional groups (BPDI), which are torsionally flexible and capable of solid-state motion. Using ditopic and tritopic hydrogen-bond donor molecules, the components self-assemble through hydroxyl-pyridine synthons, and unexpectedly, all cocrystals assemble into one-dimensional hydrogen-bonded chains. In the ditopic hydrogenbonded cocrystals BPDI crystallizes in a nearly planar geometry, while in the tritopic hydrogenbonded cocrystals, BPDI exhibits significant twisting. One of the tritopic donors is also conformationally flexible and capable of solid-state motion, and although motion was not observed in the donor, motion was induced in half of the **BPDI**. The motion and twisting resulted in higher TE behavior along the direction of motion, among other cocrystals that were discussed here. The effect of twisting in **BPDI** molecules in tritopic cocrystals affected the X₂ and X₃ principal axes. From the above reported cases, controlling the torsional flexibility in imine-based molecules is challenging; however, achieving significant twisting along with molecular pedal motion in imines can result in large TE behavior in the materials. We are continuing to investigate the predictability of motion and torsional flexibility in imine-containing molecules as a path to controlling TE behaviors in these materials.

ASSOCIATED CONTENT

Supporting Information. Experimental procedures, variable temperature single-crystal X-ray

data, powder X-ray diffraction data, thermal expansion data, NMR spectra, crystal structures,

and variation of unit cell parameters with temperature.

Accession Codes. CCDC 2212445-2212468 and 2212605-2212610 contain the supplementary

crystallographic data for this paper. These data can be obtained free of charge via

www.ccdc.cam.ac.uk/structures.

AUTHOR INFORMATION

Corresponding Author

*Email: kristin.hutchins@ttu.edu

Author Contributions

The manuscript was written through contributions of all authors. All authors have given approval

to the final version of the manuscript.

ACKNOWLEDGMENT

KMH gratefully acknowledges financial support from the National Science Foundation DMR-

2045506.

REFERENCES

(1) Gunawardana, C. A.; Aakeröy, C. B. Co-crystal synthesis: fact, fancy, and great expectations.

Chem. Commun. 2018, 54, 14047-14060.

17

- (2) Duggirala, N. K.; LaCasse, S. M.; Zaworotko, M. J.; Krzyzaniak, J. F.; Arora, K. K. Pharmaceutical cocrystals: Formulation approaches to develop robust drug products. *Cryst. Growth Des.* **2020**, *20*, 617-626.
- (3) Sathisaran, I.; Dalvi, S. V. Engineering cocrystals of poorly water-soluble drugs to enhance dissolution in aqueous medium. *Pharmaceutics* **2018**, *10*, 108.
- (4) Vainauskas, J.; Topić, F.; Bushuyev, O. S.; Barrett, C. J.; Friščić, T. Halogen bonding to the azulene π-system: cocrystal design of pleochroism. *Chem. Commun.* **2020**, *56*, 15145-15148.
- (5) Yousef, M. A. E.; Vangala, V. R. Pharmaceutical cocrystals: Molecules, crystals, formulations, medicines. *Cryst. Growth Des.* **2019**, *19*, 7420-7438.
- (6) Hutchins, K. M.; Groeneman, R. H.; Reinheimer, E. W.; Swenson, D. C.; MacGillivray, L. R. Achieving dynamic behaviour and thermal expansion in the organic solid state via cocrystallization. *Chem. Sci.* **2015**, *6*, 4717-4722.
- (7) Hutchins, K. M.; Kummer, K. A.; Groeneman, R. H.; Reinheimer, E. W.; Sinnwell, M. A.; Swenson, D. C.; MacGillivray, L. R. Thermal expansion properties of three isostructural cocrystals composed of isosteric components: interplay between halogen and hydrogen bonds. *CrystEngComm* **2016**, *18*, 8354-8357.
- (8) Bushuyev, O. S.; Friščić, T.; Barrett, C. J. Controlling dichroism of molecular crystals by cocrystallization. *Cryst. Growth Des.* **2016**, *16*, 541–545.
- (9) Bushuyev, O. S.; Corkery, T. C.; Barrett, C. J.; Friščić, T. Photo-mechanical azobenzene cocrystals and in situ X-ray diffraction monitoring of their optically-induced crystal-to-crystal isomerisation. *Chem. Sci.* **2014**, *5*, 3158-3164.

- (10) Hall, A. V.; Yufit, D. S.; Apperley, D. C.; Senak, L.; Musa, O. M.; Hood, D. K.; Steed, J. W. The crystal engineering of radiation-sensitive diacetylene cocrystals and salts. *Chem. Sci.* **2020**, *11*, 8025-8035.
- (11) Savchenkov, A. V.; Vologzhanina, A. V.; Pushkin, D. V.; Serezhkina, L. B.; Serezhkin, V. N. Highly conjugated systems with pedal motion in uranyl crotonate compounds with 1,2-bis(4-pyridyl)ethylene as a neutral ligand or a counter cation. *Inorg. Chim. Acta* **2019**, *498*, 119089.
- (12) Majerz, I.; Sawka-Dobrowolska, W.; Sobczyk, L. Structure and spectroscopic behaviour of the solid adduct of 3-methylpyridine with 2,6-dichloro-4-nitrophenol. *J. Mol. Struct.* **1993**, *297*, 177-184.
- (13) Majerz, I.; Malarski, Z.; Sobczyk, L. Proton transfer and correlations between the C-O, O-H, N-H and O···N bond lengths in amine phenolates. *Chem. Phys. Lett.* **1997**, *274*, 361-364.
- (14) Steiner, T.; Majerz, I.; C.Wilson, C. First O-H-N hydrogen bond with a centered proton obtained by thermally induced proton migration. *Angew. Chem. Int. Ed.* **2001**, *40*, 2651-2654.
- (15) Schmidtmann, M.; Wilson, C. C. Hydrogen transfer in pentachlorophenol-dimethylpyridine complexes. *CrystEngComm* **2008**, *10*, 177-183.
- (16) Shattock, T. R.; Arora, K. K.; Vishweshwar, P.; Zaworotko, M. J. Hierarchy of supramolecular synthons: Persistent carboxylic acid···pyridine hydrogen bonds in cocrystals that also contain a hydroxyl moiety. *Cryst. Growth Des.* **2008**, *8*, 4533-4545.
- (17) Mukherjee, A.; Desiraju, G. R. Combinatorial exploration of the structural landscape of acid-pyridine cocrystals. *Cryst. Growth Des.* **2014**, *14*, 1375-1385.

- (18) Lemmerer, A.; Adsmond, D. A.; Esterhuysen, C.; Bernstein, J. Polymorphic co-crystals from polymorphic co-crystal formers: Competition between carboxylic acid···pyridine and phenol···pyridine hydrogen bonds. *Cryst. Growth Des.* **2013**, *13*, 3935-3952.
- (19) Řezáč, J.; Riley, K. E.; Hobza, P. S66: A Well-balanced database of benchmark interaction energies relevant to biomolecular structures. *J. Chem. Theory Comput.* **2011**, *7*, 2427-2438.
- (20) Dunitz, J. D.; Gavezzotti, A. Supramolecular synthons: Validation and ranking of intermolecular interaction energies. *Cryst. Growth Des.* **2012**, *12*, 5873-5877.
- (21) Li, T.; Zhou, P.; Mattei, A. Electronic origin of pyridinyl N as a better hydrogen-bonding acceptor than carbonyl O. *CrystEngComm* **2011**, *13*, 6456-6360.
- (22) Vener, M. V.; Levina, E. O.; Koloskov, O. A.; Rykounov, A. A.; Voronin, A. P.; Tsirelson, V. G. Evaluation of the lattice energy of the two-component molecular crystals using solid-state density functional theory. *Cryst. Growth Des.* **2014**, *14*, 4997-5003.
- (23) Trita, A. S.; Roisnel, T.; Mongin, F.; Chevallier, F. Hydrogen bond templated 1:1 macrocyclization through an olefin metathesis/hydrogenation sequence. *Org. Lett.* **2013**, *15*, 3798-3801.
- (24) Khan, M.; Enkelmann, V.; Brunklaus, G. O-H···N heterosynthon: A robust supramolecular unit for crystal engineering. *Cryst. Growth Des.* **2009**, *9*, 2354-2362.
- (25) Chu, Q.; Duncan, A. J. E.; Papaefstathiou, G. S.; Hamilton, T. D.; Atkinson, M. B. J.; Mariappan, S. V. S.; MacGillivray, L. R. Putting cocrystal stoichiometry to work: A reactive hydrogen-bonded "superassembly" enables nanoscale enlargement of a metal-organic rhomboid via a solid-state photocycloaddition. *J. Am. Chem. Soc.* **2018**, *140*, 4940-4944.

- (26) Bučar, D.-K.; Sen, A.; Mariappan, S. V. S.; MacGillivray, L. R. A [2+2] cross-photodimerisation of photostable olefins via a three-component cocrystal solid solution. *Chem. Commun.* **2012**, *48*, 1790-1792.
- (27) MacGillivray, L. R.; Reid, J. L.; Ripmeester, J. A. Supramolecular control of reactivity in the solid state using linear molecular templates. *J. Am. Chem. Soc.* **2000**, *122*, 7817-7818.
- (28) Balszuweit, J.; Blanke, M.; Saccone, M.; Mezger, M.; Daniliuc, C. G.; Wölper, C.; Giese, M.; Voskuhl, J. Naturally occurring polyphenols as building blocks for supramolecular liquid crystals substitution pattern dominates mesomorphism. *Mol. Syst. Des. Eng.* **2021**, *6*, 390-397.
- (29) Hosseini, M. W. Molecular tectonics: from molecular recognition of anions to molecular networks. *Coord. Chem. Rev.* **2003**, *240*, 157-166.
- (30) Long, S.; Li, T. Controlled formation of the acid-pyridine heterosynthon over the acid-acid homosynthon in 2-anilinonicotinic acids. *Cryst. Growth Des.* **2009**, *9*, 4993-4997.
- (31) Ding, X.; Unruh, D. K.; Groeneman, R. H.; Hutchins, K. M. Controlling thermal expansion within mixed cocrystals by tuning molecular motion capability. *Chem. Sci.* **2020**, *11*, 7701-7707.
- (32) Hutchins, K. M.; Unruh, D. K.; Verdu, F. A.; Groeneman, R. H. Molecular pedal motion influences thermal expansion properties within isostructural hydrogen-bonded co-crystals. *Cryst. Growth Des.* **2018**, *18*, 566-570.
- (33) Kumar, S.; Priyasha; Das, D. Molecular tiltation and supramolecular interactions induced uniaxial NTE and biaxial PTE in bis-imidazole-based co-crystals. *New J. Chem.* **2022**, *46*, 18465-18470.

- (34) Bhattacharya, S.; Saha, B. K. Interaction Dependence and Similarity in Thermal Expansion of a Dimorphic 1D Hydrogen-Bonded Organic Complex. *Cryst. Growth Des.* **2013**, *13*, 3299–3302.
- (35) Das, D.; Jacobs, T.; Barbour, L. J. Exceptionally large positive and negative anisotropic thermal expansion of an organic crystalline material. *Nat. Mater.* **2010**, *9*, 36-39.
- (36) Miller, W.; Smith, C. W.; Mackenzie, D. S.; Evans, K. E. Negative thermal expansion: a review. *J. Mater. Sci.* **2009**, *44*, 5441-5451.
- (37) Barrera, G. D.; Bruno, J. A. O.; Barron, T. H. K.; Allan, N. L. Negative thermal expansion. J. Phys.: Condens. Matter 2005, 17, R217-R252.
- (38) Dutta, S.; Vikas; Thangavel, V.; Munshi, P. Ferroelectricity and uniaxial negative thermal expansion in a purely organic multifunctional material. *ACS Appl. Electron. Mater.* **2021**, *3*, 3633-3640.
- (39) Goodwin, A. L.; Calleja, M.; Conterio, M. J.; Dove, M. T.; Evans, J. S. O.; Keen, D. A.; Peters, L.; Tucker, M. G. Colossal positive and negative thermal expansion in the framework material Ag ₃[Co(CN)₆]. *Science* **2008**, *319*, 794-797.
- (40) Braga, D.; Grepioni, F.; Maini, L.; d'Agostino, S. From solid-state structure and dynamics to crystal engineering. *Eur. J. Inorg. Chem.* **2018**, *2018*, 3597-3605.
- (41) Yao, Z.-S.; Guan, H.; Shiota, Y.; He, C.-T.; Wang, X.-L.; Wu, S.-Q.; Zheng, X.; Su, S.-Q.; Yoshizawa, K.; Kong, X.; et al. Giant anisotropic thermal expansion actuated by thermodynamically assisted reorientation of imidazoliums in a single crystal. *Nat. Commun.* **2019**, *10*, 4805.

- (42) Panda, M. K.; Runčevski, T.; Chandra Sahoo, S.; Belik, A. A.; Nath, N. K.; Dinnebier, R. E.; Naumov, P. Colossal positive and negative thermal expansion and thermosalient effect in a pentamorphic organometallic martensite. *Nat. Commun.* **2014**, *5*, 4811.
 - (43) Harada, J.; Ogawa, K. Pedal motion in crystals. *Chem. Soc. Rev.* **2009**, *38*, 2244-2252.
- (44) Harada, J.; Ogawa, K. Invisible but common motion in organic crystals: A pedal motion in stilbenes and azobenzenes. *J. Am. Chem. Soc.* **2001**, *123*, 10884-10888.
- (45) Juneja, N.; Unruh, D. K.; Bosch, E.; Groeneman, R. H.; Hutchins, K. M. Effects of dynamic pedal motion and static disorder on thermal expansion within halogen-bonded co-crystals. *New J. Chem.* **2019**, *43*, 18433-18436.
- (46) Park, I.-H.; Medishetty, R.; Lee, H.-H.; Mulijanto, C. E.; Quah, H. S.; Lee, S. S.; Vittal, J. J. Formation of a syndiotactic organic polymer inside a MOF by [2+2] photo-polymerization reaction. *Angew. Chem. Int. Ed.* **2015**, *54*, 7313-7317.
- (47) Juneja, N.; Shapiro, N. M.; Unruh, D. K.; Bosch, E.; Groeneman, R. H.; Hutchins, K. M. Controlling Thermal Expansion in Supramolecular Halogen-Bonded Mixed Cocrystals through Synthetic Feed and Dynamic Motion. *Angew. Chem. Int. Ed.* **2022**, e202202708.
- (48) King, N. R.; Whale, E. A.; Davis, F. J.; Gilbert, A.; Mitchell, G. R. Effect of media polarity on the photoisomerisation of substituted stilbene, azobenzene and imine chromophores. *J. Mater. Chem.* **1997**, *7*, 625-630.
- (49) Harada, J.; Harakawa, M.; Ogawa, K. Conformational change of N-benzylideneanilines in crystals. *Acta Cryst.* **2004**, *B60*, 589-597.

- (50) Lan, L.; Di, Q.; Li, L.; Liu, B.; Yu, X.; Naumov, P. e.; Zhang, H. Packing-dependent mechanical properties of schiff base crystals. *Cryst. Growth Des.* **2022**, *22*, 3435-3441.
- (51) Harada, J.; Harakawa, M.; Ogawa, K. Torsional vibration and central bond length of N-benzylideneanilines. *Acta Cryst.* **2004**, *B60*, 578-588.
- (52) Bürgi, H. B.; Dunitz, J. D. Molecular conformation of benzylideneanilines; relation to electronic structure and spectra. *J. Chem. Soc. D* **1969**, 472-473.
- (53) Juneja, N.; Zahid, E.; Unruh, D. K.; Hutchins, K. M. Solid-state behaviors of imines: colossal biaxial positive thermal expansion, motion capability, and phase transitions. *CrystEngComm* **2021**, *23*, 4439-4443.
- (54) Kaur, M.; Yusuf, M.; Malik, A. K. Synthesis of copper metal organic framework based on schiff base tricarboxylate ligand for highly selective and sensitive detection of 2,4,6-Trinitrophenol in aqueous medium. *J Fluoresc.* **2021**, *31*, 1959-1973.
- (55) Cheng, Y.-W.; Huang, W.-Y.; Ho, K.-S.; Hsieh, T.-H.; Jheng, L.-C.; Kuo, Y.-M. Fe, N-doped metal organic framework prepared by the calcination of iron chelated polyimines as the cathode-catalyst of proton exchange membrane fuel cells. *Polymers* **2021**, *13*, 3850.
- (56) Ji, W.; Hamachi, L. S.; Natraj, A.; Flanders, N. C.; Li, R. L.; Chen, L. X.; Dichtel, W. R. Solvothermal depolymerization and recrystallization of imine-linked two-dimensional covalent organic frameworks. *Chem. Sci.* **2021**, *12*, 16014-16022.
- (57) Wang, S.; Chavez, A. D.; Thomas, S.; Li, H.; Flanders, N. C.; Sun, C.; Strauss, M. J.; Chen, L. X.; Markvoort, A. J.; Bredas, J.-L.; et al. Pathway complexity in the stacking of imine-linked

macrocycles related to two-dimensional covalent organic frameworks. *Chem. Mater.* **2019**, *31*, 7104-7111.

- (58) Li, R. L.; Flanders, N. C.; Evans, A. M.; Ji, W.; Castano, I.; Chen, L. X.; Gianneschi, N. C.; Dichtel, W. R. Controlled growth of imine-linked two-dimensional covalent organic framework nanoparticles. *Chem. Sci.* **2019**, *10*, 3796-3801.
- (59) Cortés-Guzmán, K. P.; Parikh, A. R.; Sparacin, M. L.; Remy, A. K.; Adegoke, L.; Chitrakar, C.; Ecker, M.; Voit, W. E.; Smaldone, R. A. Recyclable, biobased photoresins for 3D printing through dynamic imine exchange. *ACS Sustainable Chem. Eng.* **2022**, *10*, 13091-13099.
- (60) Jaime-Adán, E.; Germán-Acacio, J. M.; Toscano, R. A.; Hernández-Ortega, S.; Valdés-Martínez, J. Imine-benzoic acid cocrystals as a tool to study intermolecular interactions in schiff bases. *Cryst. Growth Des.* **2020**, *20*, 2240-2250.
- (61) Sanii, R.; Bajpai, A.; Patyk-Kaźmierczak, E.; Zaworotko, M. J. High Yield, Low-Waste Synthesis of a Family of Pyridyl and Imidazolyl-Substituted Schiff Base Linker Ligands. *ACS Sustainable Chem.* **2018**, *6*, 14589-14598.
- (62) Q.-F. Hou, L. Y. a. S.-M. J. *N,N*-Bis(4-pyridylmethyl-ene)benzene-1,4-diamine. *Acta Cryst.* **2007**, *E63*, 939-940.
- (63) Bajpai, A.; Scott, H. S.; Pham, T.; Chen, K.-J.; Space, B.; Lusi, M.; Perry, M. L.; Zaworotko, M. J. Towards an understanding of the propensity for crystalline hydrate formation by molecular compounds. *IUCrJ* **2016**, *3*, 430-439.

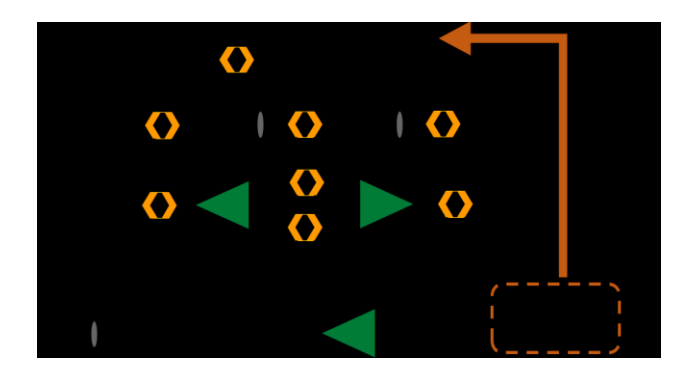
- (64) Elacqua, E.; Kaushik, P.; Groeneman, R. H.; Sumrak, J. C.; Bucar, D.; MacGillivray, L. R. A Supramolecular protecting group strategy introduced to the organic solid state: Enhanced reactivity through molecular pedal motion. *Angew. Chem. Int. Ed.* **2011**, *51*, 1037-1041.
- (65) Weyna, D. R.; Shattock, T.; Vishweshwar, P.; Zaworotko, M. J. Synthesis and structural characterization of cocrystals and pharmaceutical cocrystals: Mechanochemistry vs slow evaporation from solution. *Cryst. Growth Des.* **2008**, *9*, 1106-1123.
- (66) Ravat, P.; SeethaLekshmi, S.; Biswas, S. N.; Nandy, P.; Varughese, S. Equivalence of ethylene and azo-bridges in the modular design of molecular complexes: Role of weak interactions. *Cryst. Growth Des.* **2015**, *15*, 2389-2401.
- (67) Papaefstathiou, G. S.; MacGillivray, L. R. Discrete versus infinite molecular self-assembly: Control in crystalline hydrogen-bonded assemblies based on resorcinol. *Org. Lett.* **2001**, *3*, 3835-3838.
- (68) Biradha, K.; Zaworotko, M. J. A Supramolecular analogue of cyclohexane sustained by aromatic C-H···π interactions: Complexes of 1,3,5-Trihydroxybenzene with substituted pyridines. *J. Am. Chem. Soc.* **1998**, *120*, 6431-6432.
- (69) Cvetkovski, A.; Bertolasi, V.; Ferretti, V. Supramolecular hydrogen-bonding patterns of cocrystals containing the active pharmaceutical ingredient (API) phloroglucinol and N-heterocycles. *Acta Cryst.* **2016**, *B60*, 326-334.
- (70) Mapp, L. K.; Coles, S. J.; Aitipamula, S. Design of cocrystals for molecules with limited hydrogen bonding functionalities: Propyphenazone as a model system. *Cryst. Growth Des.* **2017**, 17, 163-174.

- (71) Guo, C.; Zhang, Q.; Zhu, B.; Zhang, Z.; Ma, X.; Dai, W.; Gong, X.; Ren, G.; Mei, X. Drug-Drug cocrystals provide significant improvements of drug properties in treatment with progesterone. *Cryst. Growth Des.* **2020**, *20*, 3053-3063.
- (72) He, H.; Zhang, Q.; Li, M.; Wang, J.-R.; Mei, X. Modulating the dissolution and mechanical properties of resveratrol by cocrystallization. *Cryst. Growth Des.* **2017**, *17*, 3989-3996.
- (73) Chadha, R.; Dureja, J.; Karan, M. Tempering trans-resveratrol from the molecule to crystal level: A contemporary approach toward polymorphic pursuits and morphological insights. *Cryst. Growth Des.* **2016**, *16*, 605-616.
- (74) Peng, B.; He, H.; Li, M.; Wang, J.-R.; Mei, X. Comparison of the crystal structures and physicochemical properties of novel resveratrol cocrystals. *Acta Cryst.* **2019**, *B75*, 1186-1196.
- (75) Cliffe, M. J.; Goodwin, A. L. PASCal: a principal axis strain calculator for thermal expansion and compressibility determination. *J. Appl. Cryst.* **2012**, *45*, 1321–1329

For Table of Contents Only

Impact of Torsional and Conformational Flexibility on Pedal Motion and Thermal Expansion in Pyridyl Bisimine Cocrystals

Navkiran Juneja, Daniel K. Unruh, Gary C. George III, and Kristin M. Hutchins



Synopsis: A torsionally-flexible bipyridine containing two imine groups was cocrystallized with ditopic and tritopic hydrogen-bond donor molecules, and the components self-assemble into one-dimensional chains. When a torsionally-flexible donor molecule is used, molecular pedal motion is achieved in the bipyridine molecule accompanied by the largest uniaxial thermal expansion coefficient within the series.